

The Öhman Effect: Line Profile Polarization in Hot and Cool Stars

J. Patrick Harrington¹

1. Continuum Polarization from Stellar Atmospheres

The continuum radiation emerging from a stellar atmosphere will in general be slightly polarized due to the scattering component of the extinction. This polarization varies with the angle between the emergent ray and the normal to the surface, and is greatest near the stellar limb.

Chandrasekhar (1946, 1960) solved the radiative transfer equations including polarization for a plane-parallel atmosphere with opacity due entirely to scattering according to a Rayleigh (dipole) phase function. This was thought to be relevant to a hot stellar atmosphere where electron scattering can be the main opacity source. This solution is independent of wavelength and results in a maximum polarization at the limb of 11.7%. Unfortunately, *pure* electron scattering opacity is not realistic for hot stars. The appropriate equations for a mixture of scattering and absorption were formulated by Code (1950), who considered atmospheres with a constant ratio of scattering to absorption. He showed that the degree of polarization depended upon (i) the ratio of scattering to absorption, and (ii) the gradient of the source function with depth in the atmosphere. The gradient of the source function depends strongly on the wavelength – the gradient of the Planck function with temperature is much smaller at long wavelengths compared to wavelengths near the peak of the Planck function – and thus the polarization from a hot star at visual wavelengths will be much smaller than Chandrasekhar’s pure scattering result.

Harrington (1969) suggested that there could be substantial polarization from the atmospheres of cool stars, due to the Rayleigh scattering by molecular hydrogen. In cool stars the gradient of the source function is steep at visual wavelengths, and his solutions showed that the polarization might actually exceed that of the Chandrasekhar pure scattering case.

This early work was not based upon realistic model atmospheres. We now have programs which calculate the structure of atmospheres for a full range of effective temperatures, gravities and chemical compositions. But polarization of the emergent radiation is generally neglected in such programs – the scattering is normally assumed to be isotropic. This is because there is little difference in limb darkening computed with the assumption of isotropic scattering compared to a model where the true dipole phase function is used. As regards the polarization, for an unresolved spherical star, symmetry will cause it to cancel completely (any limb region will have an identical region oriented at a right angle to it) so that it is of no observational interest.

Recently, however, the interest in exoplanets have prompted a reconsideration of stellar

¹Department of Astronomy, University of Maryland, College Park, MD

polarization. The transit of an exoplanet breaks the spherical symmetry of the star thus gives rise to a polarization signature (e.g., Carciofi and Magalhães, 2005). This signal, diluted by the whole stellar flux, will be very small (a fractional polarization of $\sim 10^{-5}$), but could reveal important information about the exoplanet orbit. At the same time, there is great interest in the detection of the polarization signal from starlight that is scattered by the atmosphere of a “hot Jupiter”, so it is likely that there will be efforts to achieve the highest possible accuracy in polarization measurements. It is thus useful to have computations of the polarization expected for a variety of realistic stellar atmospheres. Some results have been presented by Kostogryz and Berdyugina (2015). To avoid recomputing model atmospheres, Harrington (2015) used tabulated models for both hot and cool stars. This is possible if the tabulated models include both the scattering and the monochromatic continuum absorption as a function of depth. Harrington² presents results at 28 wavelengths for 52 hot stellar models (15,000K – 50,000K) and at 20 wavelengths for 438 cool star models (2500K – 6000K). More recently, Kostogryz et al. (2016) have obtained results for stars with extended, spherical atmospheres.

Such calculations show that the amount of polarization depends, firstly, upon the effective temperature of the star. To have a source of scattering, the star must either be hot, so that opacity by free electrons is important, or cool, so that there is Rayleigh scattering by atomic hydrogen, helium or molecular hydrogen. The polarization is greater for stars of lower surface gravity due to their lower density atmospheres. For stars of intermediate temperature - solar-type stars - the continuum polarization is very small.³ A key point is that the amount of polarization depends upon the anisotropy of the radiation field near the surface ($\tau < 1$), and this in turn depends on the gradient of the Planck function. For hot stars at visible wavelengths, the radiation field is not strongly peaked outward, and the polarization is found to be quite small. Hot stars will have strong polarization in the far ultraviolet, but there are no instruments to measure polarization at these wavelengths. Cool stars do have a strong gradient of the Planck function at the blue end of the visual spectrum and thus are the most promising candidates for detection.

The purpose of this paper is to provide some results for another signature of atmospheric polarization. It is an effect that can be substantial but which only appears at high spectral resolution in stars of rather small rotational velocities.

2. The Öhman Effect

When the emergent radiation from the atmosphere of a rotating star is partially polarized, some polarization should be seen as we scan across the rotationally broadened profiles of the absorption lines in the star’s spectrum. This effect was first proposed by Öhman

²http://www.astro.umd.edu/~jph/Stellar_Polarization.html

³Continuum polarization is well measured for the sun, with levels of $\sim 0.01\%$ near the limb.

(1946). To observe the effect, it is necessary that the polarimeter be able to resolve the line, since the polarization will vanish if the radiation is averaged over the width of the line.

To see how this effect arises, consider a rotating star where the velocity of the equatorial limb is such that the Doppler shift is a few times the line width. If we look at the line center, the radiation which comes from the star’s surface along the rotation axis will show no Doppler shift, thus that intensity will be suppressed by the absorption line. We will also receive, at line center, radiation from the edges of the star near the equator, but that radiation will be red or blue shifted away from the absorption line and thus show the full continuum intensity. Now the continuum radiation from the equatorial regions is polarized parallel to the rotation axis, while the radiation from the poles is polarized perpendicular to that axis. In the absence of the absorption line, radiation from these regions would cancel so we would see no net polarization. But the absorption line suppresses the intensity from the poles, and we will see a net polarization parallel to the axis. Furthermore, radiation at the local line center from either of the equatorial regions will be shifted to the wing (as seen by a distant observer) so that contribution is suppressed. Thus the polarization from the poles will only be partly canceled. So as distant observers scan across the line, they will see polarization which swings from $-$ to $+$ to $-$ (we denote parallel polarization by $+$). Note that the polarization which appears is *continuum* polarization. The line just reveals it by blocking part of the star and breaking the spherical symmetry. *The Öhman effect has nothing to do with line polarization or the Hanle effect.*

2.1. Previous Work

I am not aware of any observations of the Öhman effect. A detailed discussion and some calculations for hot stars were presented by Collins and Cranmer (1991) and by Collins, Truax and Cranmer (1991). Collins and Cranmer present an analysis using what they term the “Struve-Unsöld model”, which is a uniformly bright rotating, spherical star with a delta-function absorption line. Based on the pure scattering solution of Chandrasekhar, they adopt a simple fit to $Q(\mu)$, the Stokes parameter of the emergent radiation, and are able to derive an analytic expression for the polarization across the rotationally broadened line. They find a peak polarization at line center of $\sim 4\%$. They also refine the model by relaxing the uniformly bright star to a model with parameterized limb darkening. The problem, as they acknowledge, is that it is essential to discard the pure scattering model and consider the emergent intensity $I(\mu)$ and Stokes $Q(\mu)$ of a realistic model atmosphere. Furthermore, one must consider the behavior of $I_\lambda(\mu)$ and $Q_\lambda(\mu)$ *within* the line, which will not in general be simply proportional to the continuum limb darkening. The point of the analytic analysis is, however, to demonstrate clearly the reality of the (non-intuitive) Öhman effect and the “ $- + -$ ” shape of the polarization profile.

Collins and Cranmer (1991) do present a realistic calculation in their paper. They use one of the model atmospheres discussed in Collins, Truax and Cranmer (1991), which are based on the ATLAS6 model atmosphere program. They consider a star of spectral type

B1 V ($T_{eff} \simeq 25,000K$, $\log g = 4$) and evaluate the effect for two wavelengths: the extreme UV Si III $\lambda 1113$ lines and the visual He I $\lambda 4026$ line. For the Si III line they find maximum Q/I of 0.004, while for the He I line in the visible part of the spectrum, the maximum effect is an underwhelming $Q/I = -4 \times 10^{-5}$. (We verify this result – see below.)

2.2. “Milne-Eddington Lines” in Model Atmospheres

As discussed in the section above, we have obtained results for the continuum limb darkening $I(\mu)$ and Stokes $Q(\mu)$ across the spectrum for a large number of both hot and cool stellar atmospheres. We would like to evaluate the Öhman effect for these stars. The proper treatment of the polarization that arises for *line* photons, where radiation is scattered in transitions between atomic or molecular levels, is a notoriously difficult problem. It involves all four Stokes parameters and the effect of the (unknown) magnetic field; substantial progress in this area has been made mainly in the case of the solar atmosphere. We will ignore the line scattering problem and treat the lines as *pure absorption* features. As justification, we note that examination of “The Second Solar Spectrum” (Gandorfer, 2002) shows that most of the features in the high resolution I/I_c and Q/I of plots of the solar limb spectrum appear to be “depolarizing”, i.e., there is a drop in the polarization at the wavelengths of the absorption lines. This implies that the spectrum can be well modeled by just adding pure LTE line absorption to the background of continuum absorption and scattering.

We will consider two approaches. The first and simplest is to take from the tabulated model atmospheres (MARCS models for cool stars and TLUSTY models for the hot stars) the run of temperature $T(\tau)$, of continuum absorption $\kappa_c(\tau)$ and of scattering $\sigma(\tau)$, as a function of monochromatic optical depth τ . From these data, we can construct what we will call a “Milne-Eddington” line. In the classical Milne-Eddington approximation, the Planck function is taken as a linear function of optical depth and the ratio of line to continuum absorption is taken as constant with optical depth. These assumptions allow an analytic solution of the transfer equation. By contrast, we will take the variation of the temperature and, most importantly, the variation of the ratio of scattering to continuous absorption, from the model atmospheres. We refer to our approach as a “Milne-Eddington” line (with quotes) because we take the ratio of line to continuum absorption to be independent of depth. Thus we replace the continuous absorption $\kappa_\lambda^c(\tau)$ with

$$\kappa_x(\tau) = \kappa_\lambda^c(\tau) [1 + r_l \phi(x)] \quad \text{and} \quad \phi(x) = \frac{1}{\sqrt{\pi}} e^{-x^2}, \quad (1)$$

where r_l is the ratio of line to continuum absorption and τ is the optical depth in the continuum at the line wavelength λ_0 . Here we assume a Doppler line profile, where x is the frequency in Doppler widths: $x = (\lambda - \lambda_0)/\Delta\lambda_D$. The Doppler width, $\Delta\lambda_D$, can be written in terms of the thermal velocity v_{th} as $\Delta\lambda_D = (\lambda_0/c) v_{th}$, and this velocity, in turn, is $v_{th} = 12.85 [T/10^4 A]^{1/2}$ km/sec. Here, A is the atomic weight of the atom (or molecule) in question. For stronger lines we may generalize $\phi(x)$ to a Voigt profile. The parameter r_l determines the line strength.

Then for each frequency x across the line profile, we compute the monochromatic optical depth in the line, τ_x , by integrating the opacity:

$$d\tau_x(\tau) = \frac{\kappa_x(\tau) + \sigma_\lambda(\tau)}{\kappa_\lambda^c(\tau) + \sigma_\lambda(\tau)} d\tau \quad (2)$$

We thus obtain the Planck function $B_\lambda[T(\tau_x)]$ and the key absorption to extinction ratio $\lambda_x(\tau_x) = \kappa_x(\tau_x)/[\kappa_x(\tau_x) + \sigma_\lambda(\tau_x)]$. We interpolate these quantities at a pre-defined grid of τ 's and solve for $I_x(\mu)$ and $Q_x(\mu)$ using finite integral transforms as outlined in Harrington (2015). Note that the limb darkening and Stokes Q_x will differ from the adjacent continuum behavior; usually, the added absorption will suppress not only Q_x but the ratio Q_x/I_x .

To keep this study as simple as possible we will assume that the stellar rotation is “slow”. As a consequence of rotation, stars increase their equatorial radius, and the surface temperature will vary with the effective surface gravity: $T_{eff} \propto g^{1/4}$. But these effects only become significant for rapidly rotating stars: e.g., for a star rotating at 1/2 its break-up velocity the increase in the equatorial radius is only 4%. Thus we will assume a spherical star with a uniform effective temperature and surface gravity.

Let the rotation axis of the star be the z-axis of a spherical coordinate system. Let θ be the angle measured from the z-axis (the co-latitude) and let ϕ be the azimuthal (longitudinal) angle measured from the direction to the observer. The velocity of any point on the stellar surface is given by $v(\theta) = v_0 \sin \theta$, where v_0 is the rotational velocity of the stellar equator. The component of this velocity seen by a distant observer is given by

$$v_{obs} = v_0 \sin \theta \sin \phi \sin i, \quad (3)$$

where i is the angle between the rotation axis and the direction of the observer. This velocity will produce a Doppler shift of $\Delta\lambda = \lambda v_{obs}/c$. Thus the Doppler shift at a given point on the stellar surface can be written

$$\Delta\lambda(\theta, \phi) = 3.336 \times 10^{-6} \lambda v_0 \sin i \sin \theta \sin \phi, \quad (4)$$

where λ and $\Delta\lambda$ are in Å units and v_0 is in km s⁻¹. This is the shift that we must apply to the Stokes parameters I and Q of the line profile at each point on the stellar surface. We see from equation (4) that the Doppler shift of every point is scaled by $\sin i$. Thus we need only consider the case where the inclination $i = 90^\circ$. A star with a rotational velocity of v_0 viewed at an inclination i will look exactly like a star with rotational velocity $v'_0 = v_0 \sin i$ seen at $i = 90^\circ$.

To combine the polarization from different patches on the stellar surface, we must express the local polarization with reference to a common axis, which we take to be the projection of the stellar rotation axis. Let the projection of the local normal onto the plane of the sky make an angle ξ with the z-axis. Then we need to rotate the local emergent $Q(\mu)$ clockwise (as seen traveling with the ray) through the angle ξ . Call the rotated parameters I' , Q' and U' . In the local reference frame the Stokes parameter $U = 0$, but the rotation gives rise to a non-zero U' . The equations for rotation are:

$$I'(\mu) = I(\mu), \quad Q'(\mu) = Q(\mu) \cos(2\xi), \quad U'(\mu) = Q(\mu) \sin(2\xi). \quad (5)$$

The angle ξ is given by $\tan \xi = \sin \phi \tan \theta$. While this produces a non-zero U' , we can disregard this parameter since a U' contribution from a point above the equator will be canceled exactly by the contribution from the same latitude below the equator, which will have the same Doppler shift but a value of $-U'$. The following integrals give the parameters as seen by the distant observer:

$$I_x = R^2 \int_{-\pi/2}^{\pi/2} \int_0^\pi I_x(\theta, \mu) \mu \sin \theta d\theta d\phi \quad (6)$$

and

$$Q_x = R^2 \int_{-\pi/2}^{\pi/2} \int_0^\pi Q_x(\theta, \mu) \cos(2\xi) \mu \sin \theta d\theta d\phi . \quad (7)$$

The value of $\mu(\theta, \phi)$ follows from $\mu = \sin \theta \cos \phi$. We carry out the evaluation of (6) and (7) as follows: We first specify the effective temperature and gravity of the star. From the tabulated model atmospheres we extract the values of $\kappa^c(\tau)$, $\sigma(\tau)$ and $T(\tau)$, interpolated at the selected line wavelength λ_0 , and with equations (1) and (2) we get $\tau(x_i)$ and $\lambda(x_i)$ for a grid x_i across the (half-)line profile. We solve the transfer equations for the emergent $I(x_i, \mu)$ and $Q(x_i, \mu)$ at these wavelengths for a grid of 18 μ_k , adequate for interpolation in μ . We cover the visible surface of the star with a grid of 181 points in θ and 121 points in ϕ for a total of 21901 points. For each point we evaluate the value of μ and interpolate to find the emergent $I(x_i, \theta, \phi)$ and $Q(x_i, \theta, \phi)$ profile. Using our selected equatorial rotational velocity v_0 , we Doppler-shift each profile according to the location of the grid point (eqn 4), and interpolate back to a standard x_i -grid of the distant observer. Finally, we sum these Stokes $I(x_i)$ and $Q(x_i)$, weighted properly, over the stellar surface.

Let us consider a MARCS model atmosphere with $T_{eff} = 4000K$ and $\log g = 3.5$ (a K4 giant). Fig. 1 shows the percent polarization, $100 \times Q(\mu)/I(\mu)$, for 11 wavelengths. For readability, we do not plot the polarization for $\mu < 0.02$ ($\sim 1^\circ$ from the limb). The magnitude of the polarization increases as we go from 6000\AA toward shorter wavelengths. At a wavelength of 4000\AA , the polarization at $\mu = 0.1$ is about -3% . (We adopt a convention where Q is negative for polarization perpendicular to the meridian.)

We now wish to evaluate the Öhman effect for a line at 4000\AA . We set the line-to-continuum ratio at $r_l = 10$, which produces a line with a central depth of $0.13 I_c$, where I_c is the continuum intensity. We consider four rotational velocities such that the equatorial Doppler shift v_0 is 1.5, 3, 6 and 10 times the Doppler width of the line. Fig. 2 shows the results. The thin black line in the left panel is the emergent flux from a point on the stellar surface in the local frame of reference. The four colored lines are $I(x)$ as given by equation (6) for the four velocities. (The values of $I(x)$ are normalized by dividing by the continuum intensity I_c .) The right panel shows the values of $100 * Q(x)$ from equation (7), again normalized by I_c . We plot this quantity to avoid the enhancement of the polarization as the intensity drops near line center. This also makes it easier to see that the area of positive Q is equal to that of negative Q .

The Öhman effect is rather small: $(Q/I_c) \simeq 3 \times 10^{-4}$ (0.03%) at line center. The effect

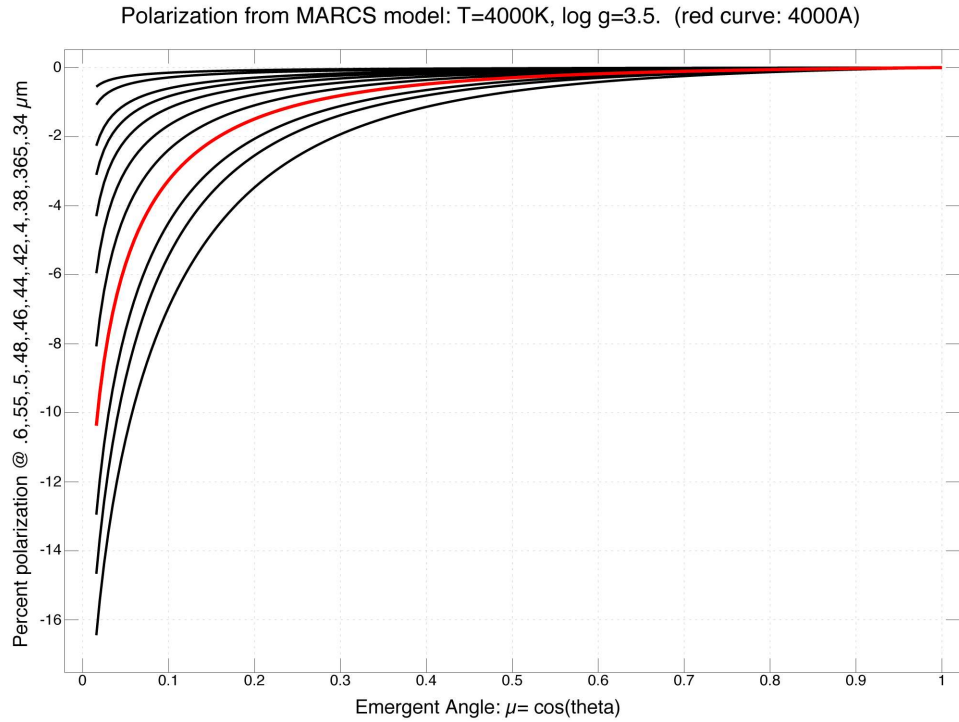


Fig. 1.— Polarization of Radiation from a MARCS model atmosphere.

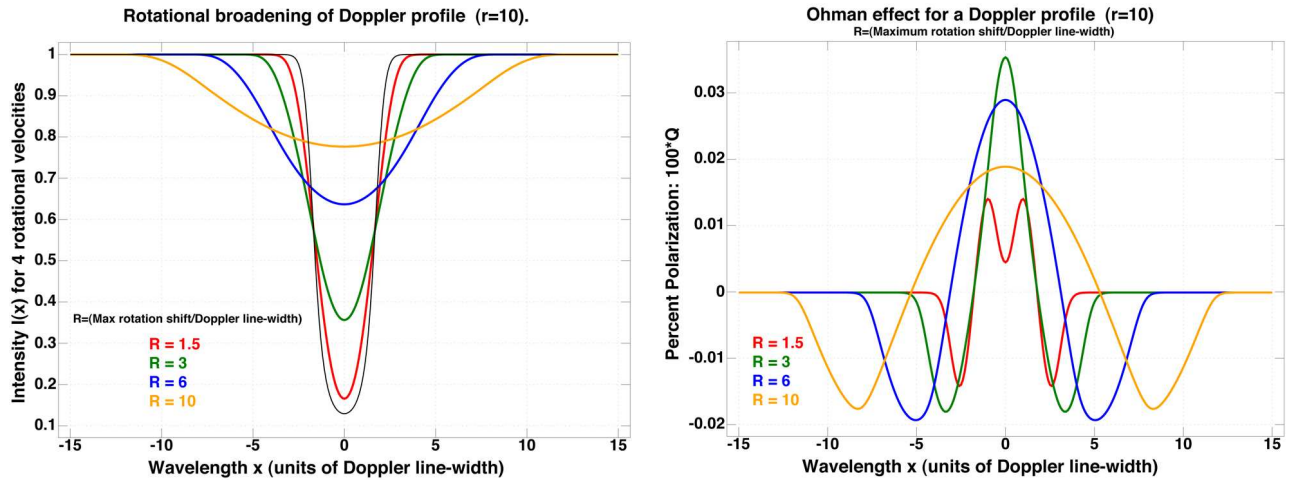


Fig. 2.— The Öhman effect for a Doppler line profile in a MARCS K4 III model atmosphere. This is a “Milne-Eddington” line with $r_l = 10$. The left panel shows the unbroadened profile (black), and after broadening by four rotational velocities. The right panel shows the polarization induced by these rotations. These results are for a stellar model with T=4000K and log g=3.5 at a central wavelength of 4000Å.

is greater at shorter wavelengths, but the flux from a 4000K star is dropping steeply towards the UV. For the case considered here, the greatest value of $Q(x)$ occurs for a rotational velocity ~ 3 Doppler widths, for which $100 * Q_x = 0.0354$ at $x = 0$. But shapes of the Q_x curves involves not only the continuum limb darkening and the center-to-limb variation of the continuum polarization, but also how this interacts with the shape of the line profile for a given rotational Doppler shift.

To disentangle these factors let us consider a totally black line with a rectangular profile: In other words, we integrate equations (6) and (7) while masking off a strip parallel to the rotation axis. The width of the strip represents the ratio of the line width to the rotation velocity. We have done this for the same stellar atmosphere and show the results in Fig. 3. The Q_x curves are similar to those of Fig 2. We should explain the dip at $x = 0$ for the $R = 1$ case. Here the rotation is so slow that the shifted line can cover the whole star, so $I_x = 0$ at $x = 0$. Thus $Q_x = 0$ there also (since $Q \leq I$). This explains the central dip in the $R = 1.5$ curve in for the Doppler profile (Fig. 2): It is due to the drop in intensity near $x = 0$; if we plot the polarization $Q(x)/I(x)$ there would be no such dip. Looking again at the $R = 1$ curves of Fig. 3, note that for this curve $I_x = 0.5$ and $Q_x = 0$ at $x = \pm 1$. That is because the sharp rectangular line covers exactly $1/2$ the stellar disk, and Q averaged over the right or left hemisphere is zero. The greatest value of Q_x occurs for $R = 2$, $\sim 0.04\%$, a bit greater than that for a ‘‘Milne-Eddington’’ Doppler line. Our rectangular line does, however, give a reasonable upper bound to the Öhman effect.

Stronger spectral lines have damping wings and are not well represented by a pure Doppler line profile. We can get an idea of their behavior by considering a Voigt profile for $\phi(x, a)$, where a is the ratio of the damping parameter Γ to the Doppler width: $a = \Gamma/4\pi\Delta\lambda_D$. We illustrate this with a stronger line, $r_l = 500$, and a large damping parameter $a = 0.1$, again at a wavelength of 4000\AA . Some results are shown in Fig. 4. The black curve in the left panel shows the unbroadened profile. The maximum value of $100 * Q$ is 0.027 , which occurs for $R = 15$. As we go to higher rotational velocities, the peak value declines. If, however, we consider the detectability of the effect, we should also look at $Q > 0$ and $Q < 0$ integrated over wavelength. We find that the integrated $|Q_x|$ continues to increase with the rotational velocity. In addition, the regions of positive and negative Q_x move further apart, so less spectroscopic resolution would be needed to detect the effect.

The magnitude of the effect will vary with the star’s effective temperature and surface gravity. In Fig. 5 we show the results for a fairly weak line, $r_l = 5$, and a ratio of Doppler shift to line width of $R = 4$. We see that the results are broadly similar for effective temperatures of 3500K, 4000K and 4500K. The magnitude of the effect increases strongly towards lower surface gravities, as that increases the continuum scattering/absorption ratio.

The wavelength of the absorption line also has a profound effect on the amount of polarization. In Fig. 6 we show results for nine wavelengths from 3400\AA to 8000\AA . The results are as expected: Because the scattering for these stars is Rayleigh scattering by atoms or molecules, it decreases strongly with wavelength, so that the effect essentially

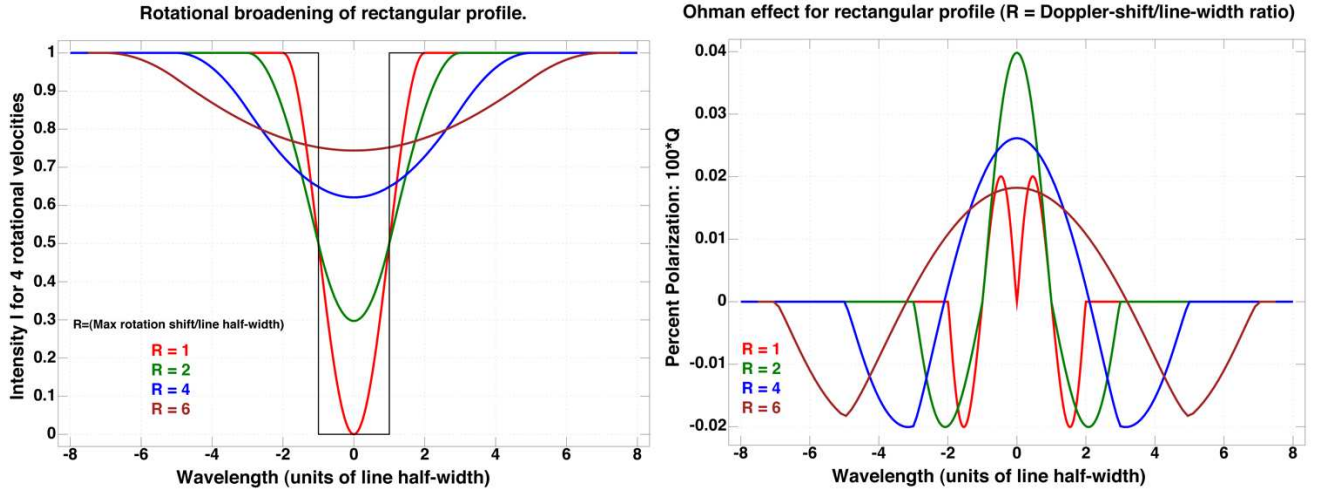


Fig. 3.— The Öhman effect for a rectangular line profile. The left panel shows the profile (black) after broadening by 4 rotational velocities. The right panel shows the polarization induced by this rotation. These results are for a stellar model with $T=4000\text{K}$ and $\log g=3.5$.

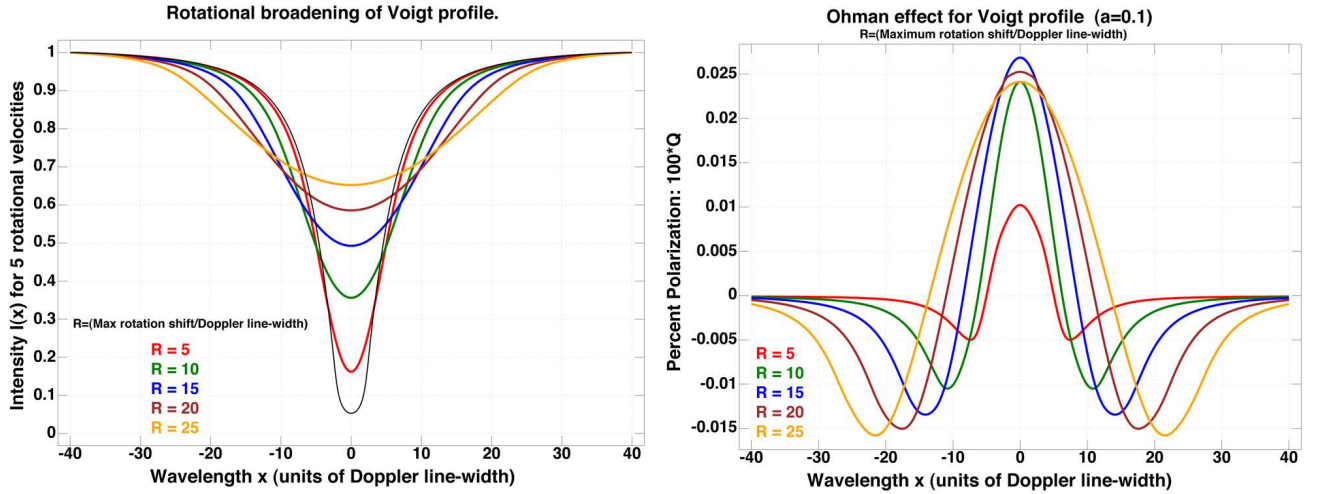


Fig. 4.— The Öhman effect for a Voigt line profile in the “Milne-Eddington” approximation with the (line/continuum) ratio $r=500$ and damping ratio $a=0.1$. The left panel shows the profile (black) after broadening by 5 different rotational velocities. The right panel shows the polarization induced by this rotation. These results are for a stellar model with $T=4000\text{K}$ and $\log g=3.5$.

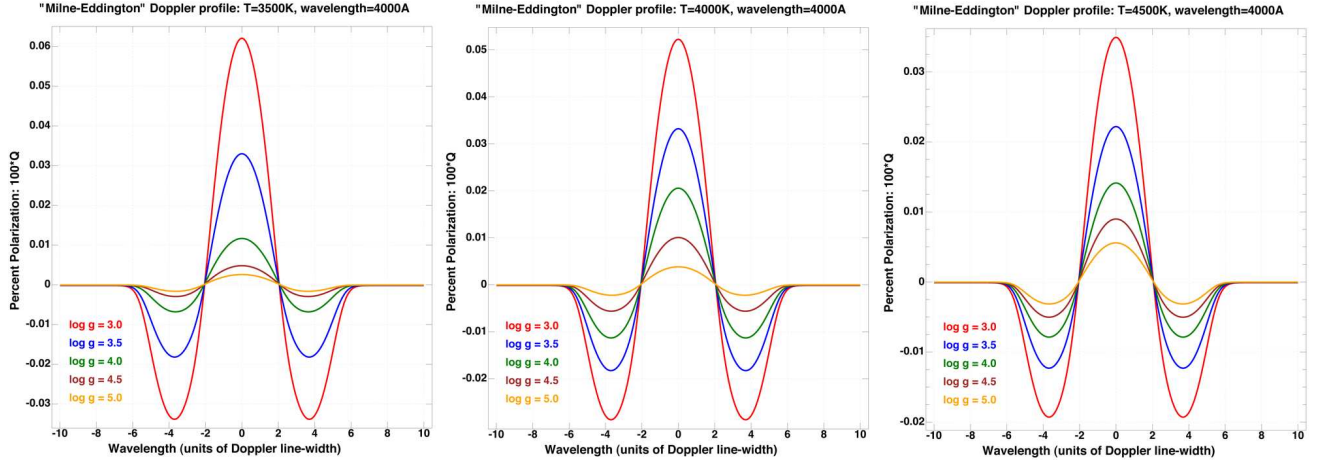


Fig. 5.— The Öhman effect for a Doppler line profile in the “Milne-Eddington” approximation with the (line/continuum) ratio $r_l = 5$ at 4000\AA . The ratio of rotational Doppler shift to Doppler line width is $R = 4$ in all cases. The panels show three effective temperatures: 3500K, 4000K and 4500K. For each temperature we show the percent polarization, $100 \times Q(x)/I_{\text{continuum}}$, for five gravities: $\log g = 5.0, 4.5, 4.0, 3.5, 3.0$. In all cases, the effect decreases with increasing surface gravity.

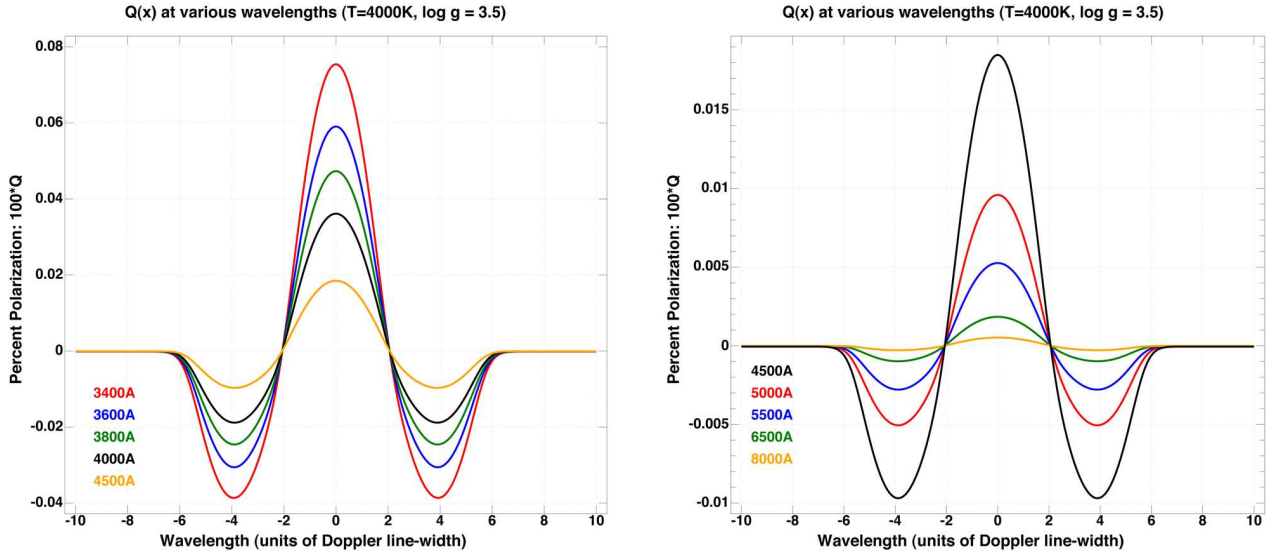


Fig. 6.— The Öhman effect for a Doppler line profile in the “Milne-Eddington” approximation with the (line/continuum) ratio $r_l = 10$ and with a ratio of rotational Doppler shift to Doppler line width of $R = 4$. Results are presented for nine wavelengths between 3400\AA and 8000\AA .

disappears at the red end of the spectrum.

2.3. The Öhman Effect for Hot Stars

Now let us consider hot stars, where the scattering is due primarily to free electrons. We may obtain the needed parameters from the stellar atmosphere code TLUSTY, if we run the code with the keyword IPOPAC=1 set. This generates a file (fort.85) with the needed continuum opacities at hundreds of wavelengths. From the opacities we can compute the monochromatic optical depths, while the electron scattering is obtained from the tabulated electron number N_e and the gas density. Then, following the same procedure as for the cool MARCS atmospheres, we can evaluate the Öhman effect for Doppler and Voigt profiles at any wavelength.

To understand the effect in hot stellar atmospheres, we should review the polarization of the emergent radiation as a function of μ at various wavelengths. In Fig. 7 we show this for a 30,000K model. We see that in the far UV (1200Å-1500Å) the polarization is substantial and negative (i.e., perpendicular to the normal). But in the visible (4000Å-6000Å) the polarization is small and, except very near the limb, is positive, with the plane parallel to the normal of the stellar surface. In the near UV (e.g. 2500Å) the polarization mixed, with the outer part of the stellar disc showing $Q(\mu) < 0$ while the center of the disc shows $Q(\mu) > 0$. This leads to very small amplitudes as well as a self-reversal of the profile in some cases (see the T=30,000K 1900Å profile in Fig. 8).

In Fig. 8 we show the results for three hot atmospheres as we range in wavelength from 1200Å to 6000Å. While we expect to see substantial polarization in the far UV – up to 0.15% at line center – the polarization in the visible is expected to be much smaller and of the opposite sense: the central peak will be negative.

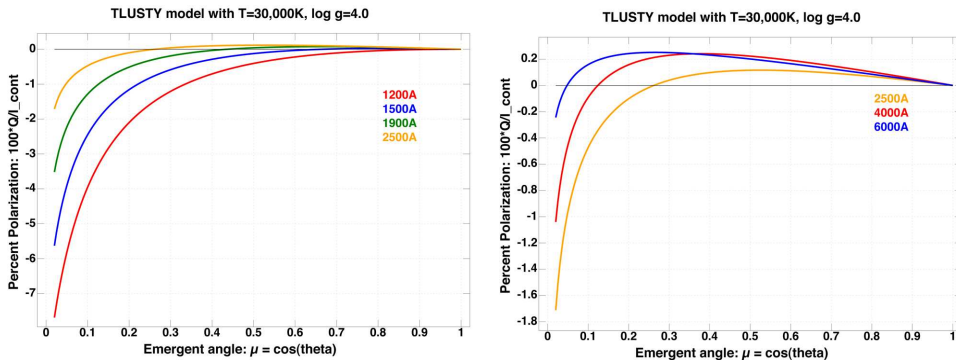


Fig. 7.— Polarization of Radiation from a hot model atmosphere. We only plot values for $\mu > 0.02$. Note that at visible wavelengths, the polarization is positive for $\mu > 0.05 - 0.13$.

2.4. Modeling the Effect in Hot Stars with a Spectrum Synthesis Code

While the foregoing results gives us an idea of the magnitude of the expected effect for stars of various temperatures and gravities as a function of wavelength, the “Milne-Eddington” model is only approximate: in reality, the line opacity will depend upon the the ionization balance of the ion or atom in question and the excitation of the atomic levels. Thus the variation of the line opacity with depth will not track the variation of the continuum absorption. The next step beyond the “Milne-Eddington” line model is to use the $I(\mu)$ and $Q(\mu)$ from a spectral synthesis program. We have provided such results (under “2nd Spectrum for some hot stars”). It is straightforward to integrate these (Doppler shifted) Stokes parameters over the surface of the rotating star to obtain the net polarization. But the resultant polarization curve would be choppy since spectral resolution of our input “2nd spectrum” is barely adequate for this sort of calculation. We have thus run the SYNSPEC spectral synthesis code at a higher resolution of 0.01\AA to obtain the input $I(\mu)$ and $Q(\mu)$.

It is interesting to compare our results with the case shown by Collins and Cranmer (1991) for the He I $\lambda 4026$ line in a B1 V star (Figure 5 of their paper). We used a TLUSTY 25000K, $\log g=4.0$ model as input to the SYNSPEC code. The result is shown in the left panel of Fig. 9. Our calculation contains weak lines on the wings of the He I line not modeled by Collins and Cranmer, and our model codes differ. Nevertheless, the results are quite similar. The central peak is negative due to the shallow gradient of the Planck function in the visible, as explained in the preceding section. The amplitude of the spread from the negative central dip to the positive peaks on either side is $Q/I = 6 \times 10^{-5}$, the same as their result. (The calculations of Collins and Cranmer include the distortion in the shape of the star due to its rotation, and this in turn induces an overall polarization of the continuum, so that their Q/I curves do not go to zero in the far wings. We do not include the change of shape of the star.)

We also include, in the right panel of Fig. 9, the result of putting a Voigt profile into a similar model atmosphere (the temperature is slightly lower) using our “Milne-Eddington” approximation: the ratio of line to continuum absorption is held constant with depth. The results are given in terms of the Doppler width, $\Delta\lambda_D$, which can be written in terms of the thermal velocity v_{th} as $\Delta\lambda_D = (\lambda_0/c) v_{th}$. This velocity, in turn, is $v_{th} = 12.85 [T/10^4 A]^{1/2}$ km/sec. Here, T is the temperature of the stellar atmosphere and A the atomic weight of the atom (or molecule) in question. For this He I line ($A=4$) at 23,000K, we have $v_{th} = 9.74$ km/s. Thus 50 km/s corresponds to $R=5$, and the line parameters for the right panel ($r_l = 1000$, $a = 0.2$, $R = 5$) were set to produce a profile similar to the synthetic spectrum line in the left panel. It can be seen that the variation of Q across the line is similar to the result in the left panel, both in shape and in magnitude.

In the far ultraviolet the polarization is much stronger and the central peaks are positive. In this part of the spectrum there is a crowding of lines, which produces a rather complex result. In Fig. 10 we show about 10\AA of spectrum around the Si IV $\lambda 1402.7$ for a 20,000K, $\log g = 3.5$ star. The projected equatorial velocity of this model has been set at 20 km/s. The

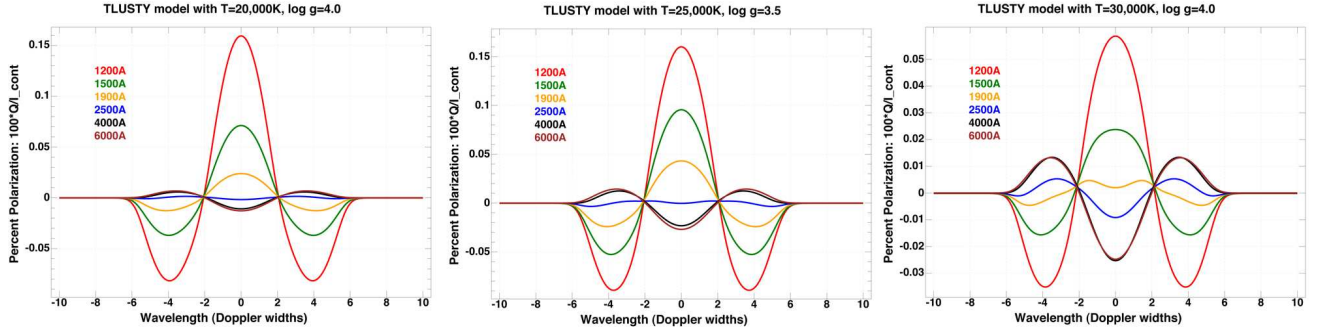


Fig. 8.— The Öhman effect for Doppler line profiles in hot stellar atmospheres at various wavelengths. We use the “Milne-Eddington” approximation with a (line/continuum) ratio of $r_l = 20$. The ratio of rotational Doppler shift to Doppler line width is $R = 4$ in all cases. The panels show three effective temperatures: 20,000K, 25,000K and 30,000K. For each temperature we show the percent polarization, $100 \times Q(x)/I_{continuum}$, across the line.

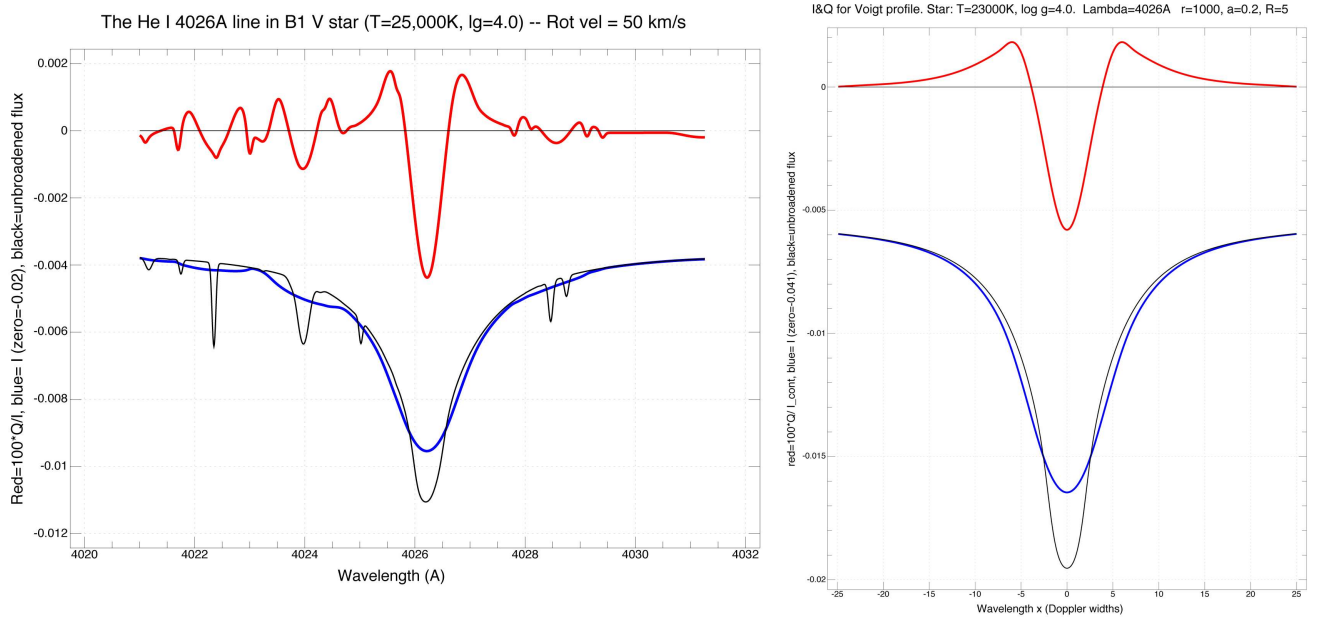


Fig. 9.— The Öhman effect for the He I 4026Å line. The left panel shows the synthetic spectrum result for comparison with Figure 5 of Collins and Cranmer (1991). The amplitude of the central dip, -4×10^{-5} , agrees with their result. The right panel is a “Milne-Eddington” Voigt profile with parameters adjusted to mimic the He I line in the left panel.

Stokes I&Q across lines of rotating star: T=20,000K, lg=3.5 -- Rot vel = 20 km/s

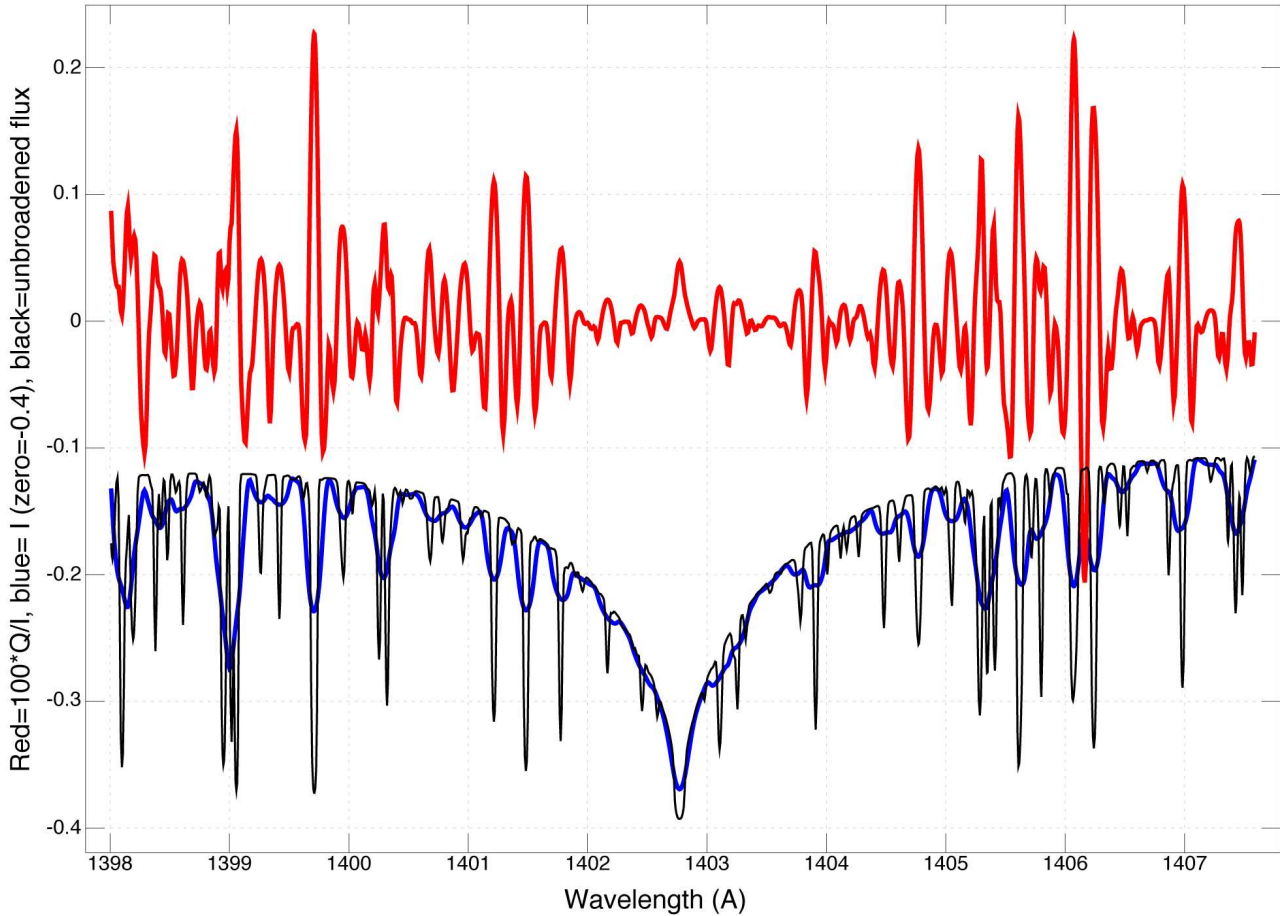


Fig. 10.— The Öhman effect for a section of synthetic stellar spectrum in the far UV. The stellar temperature is 20,000K and the log surface gravity 3.5.

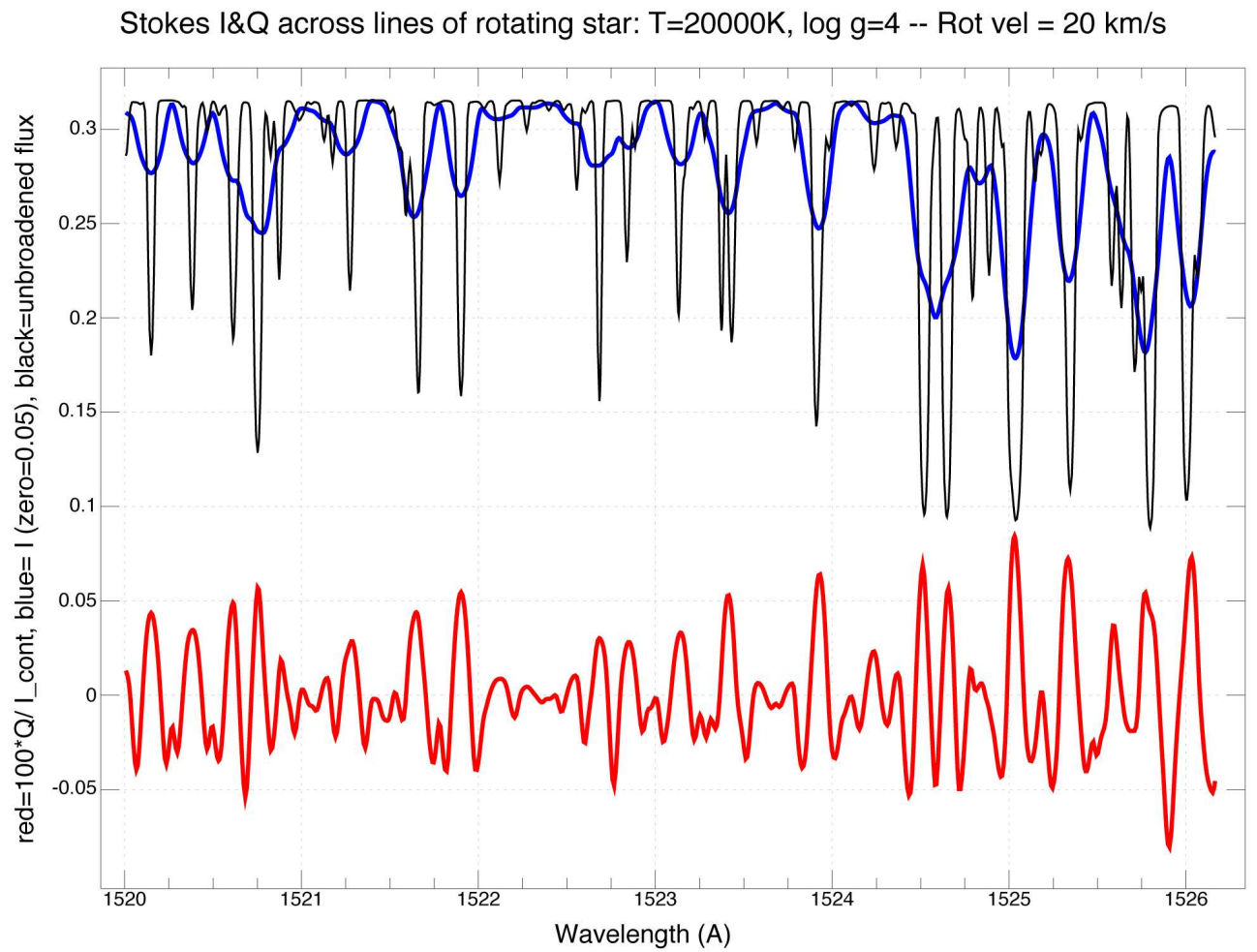


Fig. 11.— The Öhman effect a synthetic stellar spectrum near 1523Å. The stellar temperature is 20,000K and the log surface gravity 4.0.

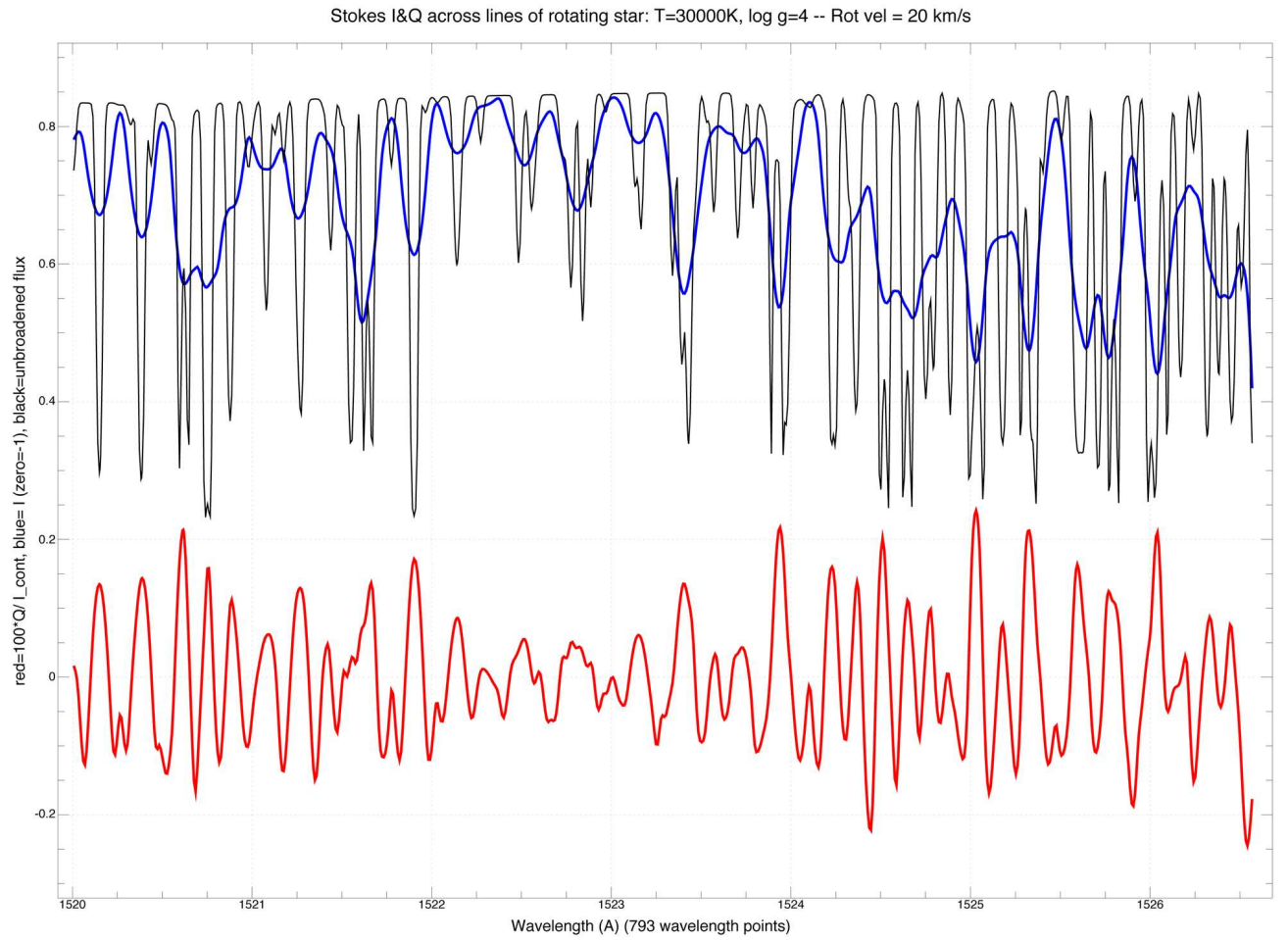


Fig. 12.— The Öhman effect a synthetic stellar spectrum near 1523Å. The stellar temperature is 30,000K and the log surface gravity 4.0.

scale on the y-axis is the percent polarization, $100*Q/I$, while below is the Doppler broadened intensity, and for comparison, the unbroadened emergent flux from the atmosphere. (The flux scale is arbitrary, scaled to fit on the figure with the polarization.) Note that the broad Si IV line produces little polarization since it is wide compared to the Doppler shifts.

2.5. The Effects of Micro- and Macroturbulence

We have presented most of our results in terms of the Doppler width of the absorption lines. The relevant line width is, however, not just the thermal Doppler width, but rather the width we would observe from an extended patch on the stellar surface. That is, the line width must include bulk motions, which are traditionally decomposed into the two limiting scales: microturbulence (motions over distances where the optical depth changes little) and macroturbulence (motions of optically thick sections of the stellar atmospheres).

2.5.1. Microturbulence

Microturbulence can be modeled by simply replacing the thermal velocity v_{th} with a velocity V defined by $V^2 = v_{th}^2 + \xi_{mic}^2$, where ξ_{mic} is the microturbulent velocity (usually a few km/sec). This simply increases the Doppler widths of all lines to $\Delta\lambda_D = (\lambda_0/c)V$. Since the Doppler width of heavy metal lines is small, e.g., 1 km/s for an iron line at 4000K (0.013\AA at 4000\AA), most lines will have a velocity V where the microturbulent width dominates the thermal broadening.

2.5.2. Macroturbulence

Macroturbulence may be larger than microturbulence however, and it cannot be treated so simply. We assume some distribution of macroturbulent velocities along the line-of-sight with the corresponding distribution of Doppler shifts $\zeta(x)$. Ideally, the macroturbulent velocity distribution would come from a hydrodynamic model of the granulation and convective motions in the stellar atmosphere, but such data is not generally available. The simplest approach is to assume that the macroturbulent velocity distribution $\zeta(x)$ is a Gaussian distribution which is independent of the viewing angle. However, observations imply that $\zeta(x)$ is not isotropic. This is discussed, e.g., in Chapter 17 of Gray (2005). A more satisfactory model seems to be one in which the motions are not turbulent, but one in which the material rises in granules, flows across them, and then descends at the granule boundaries. This implies that the motion is exclusively radial or tangential. The model assumes that the velocity distributions in both the radial and tangential directions are Gaussian with widths ζ_R and ζ_T , respectively. We let the fraction of the stellar surface where the flow is radial be A_R while the complementary area where the motion is tangential is $A_T = 1 - A_R$. Furthermore, the simplest R-T (radial-tangential) model is where $\zeta_R = \zeta_T = \zeta_{RT}$ and $A_R = A_T = 0.5$.

It might at first seem that the simplest R-T model would be equivalent to an isotropic Gaussian with width ζ_{RT} , but that is not the case. In the R-T model, at the disk center ($\mu = 1$) we see the sum of an unbroadened profile (tangential motion perpendicular to the line-of-sight) and a profile broadened by the full width ζ_{RT} (the radial motions). At the limb ($\mu = 0$), we see the same combination, this time an unbroadened profile from the radial motions and the full width ζ_{RT} from the tangential motions. However, at other positions on the disk, the profile will be different. Consider $\theta = \pi/4$ ($\mu = 1/\sqrt{2} = 0.707107$) where $\cos\theta = \sin\theta$. Then both the radial and tangential motions make a 45° angle with the line-of-sight, and both will produce the same profile, but the effective width of the Gaussian will be reduced to $\mu \zeta_{RT}$.

We have made some calculations of the Öhman effect polarization for “Milne-Eddington” lines using the simplest R-T model discussed above. The calculation proceeds as follows: For each point on the visible stellar surface, we interpolate the profiles $I(\mu)$ and $Q(\mu)$ for the μ of that point. We then broaden the profiles with the radial and tangential macroturbulent velocities of widths $\mu \zeta_{RT}$ and $\sqrt{1 - \mu^2} \zeta_{RT}$ by taking the Fourier transforms of these two Gaussians, multiplying by the transforms of the $I(\mu)$ and $Q(\mu)$ profiles, and taking the inverse Fourier transform. We then sum the two broadened I and Q profiles and apply the appropriate Doppler shift for the specific point. The Stokes Q of each point is rotated to the coordinate system aligned with the rotation axis, and the I and Q profiles are summed over the visible stellar surface.

For comparison, we have also made some models with isotropic macroturbulence. We do not find much difference in the flux profile between an R-T model and a model with isotropic Gaussian macroturbulence, where the width of the Gaussian is set to $(2/3)\zeta_{RT}$. While Fig. 17.5 of Gray (2005) shows a large difference, that is for a model with no limb darkening. We are comparing results from models where the continuum is limb-darkened and where the profile shape is also a function of the angle μ . The polarization profiles also show little difference between the isotropic and the R-T models.

We show the comparison in Fig. 13. Shown there is emergent profile of a line at 4000\AA of strength $r_l = 10$, with a Gaussian microturbulent width of unity (thin black line). This profile is then broadened by either (a) isotropic macroturbulence (orange line) or (b) simple R-T macroturbulence (yellow and purple curves). If the value of ζ_{RT} is 1.5 times the isotropic value, the results are nearly the same (orange and purple lines). These profiles are not yet broadened by rotation; the blue, green and red profiles show the result of applying a maximum rotational Doppler shift which is twice ζ_{iso} (i.e., $R=4$, 4 times the unit microturbulent width, since we have set $\zeta_{iso} = 2$). The lower panel shows the polarization that results from rotation. Note that even though the depths of the lines are reduced by macroturbulence, the polarization is not reduced proportionally (compare Fig. 2).

We have also made some calculations using R-T macroturbulence for strong lines with Voigt profiles, as in Fig. 4. There are no surprises – the polarization is almost unchanged.

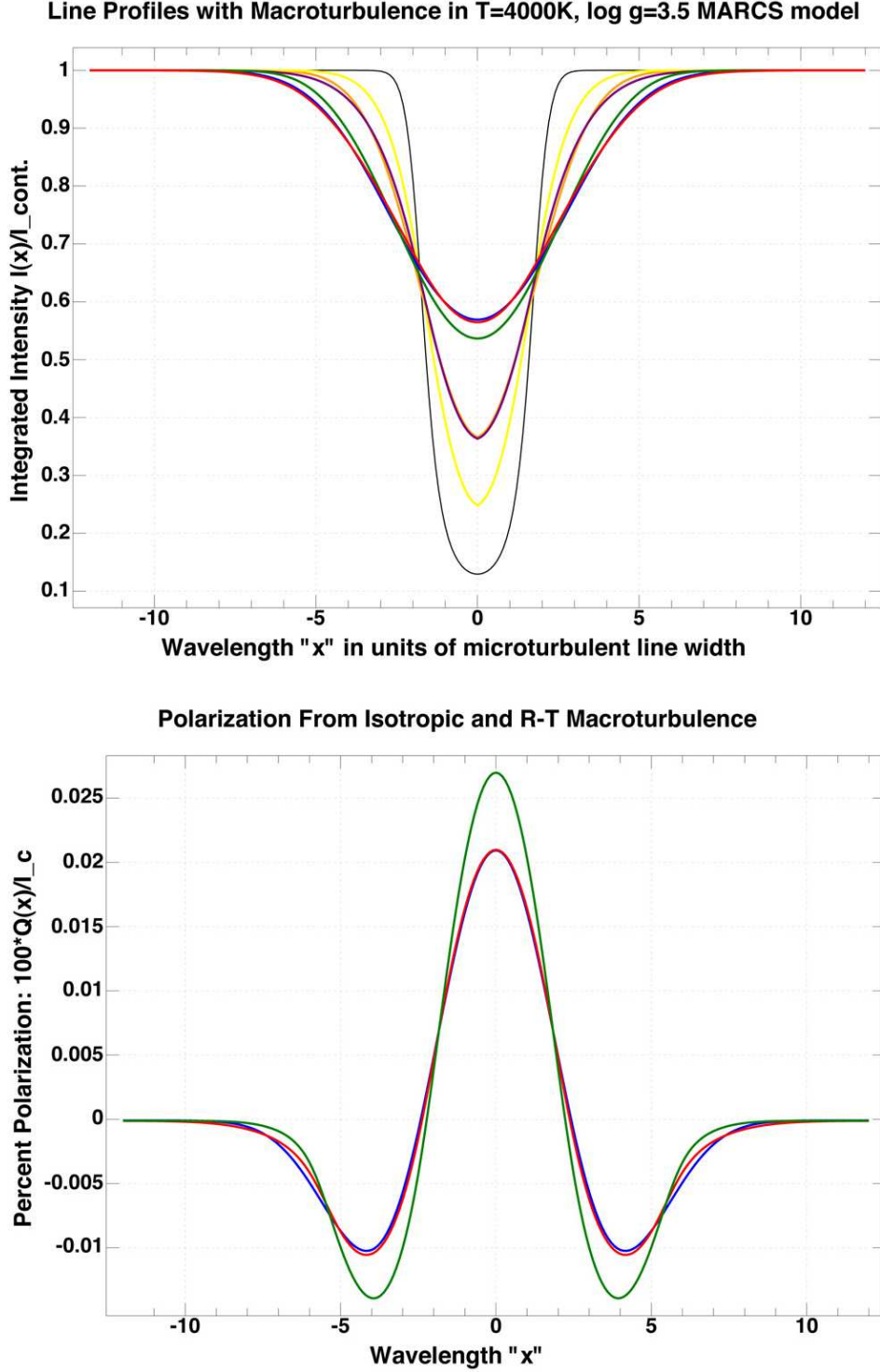


Fig. 13.— Top panel: The black line is a Milne-Eddington line with $r_l = 10$ at 4000\AA ; the only broadening is microturbulence with a width of unity. The orange line profile includes additional broadening by isotropic macroturbulence of width 2, the yellow uses R-T macroturbulence with width $\zeta_{RT} = 2$, and the purple uses $\zeta_{RT} = 3$. (The orange and purple profiles are nearly coincident.) The blue, green and red profiles are the result of applying Doppler broadening of width 4 ($R=4$) to the orange, yellow and purple profiles. Again, the isotropic macroturbulence with $\zeta_{iso} = 2$ (blue) is almost the same as R-T macroturbulence with $\zeta_{RT} = 3$ (red). Note that the equivalent widths of all these line profiles is the same. Lower panel: The Öhman effect polarization corresponding to the blue, green and red cases above.

2.6. Observability of the Effect

We have seen that the magnitude of the Öhman effect polarization is small. Coupled with the required high spectral resolution, this may make observation of the effect problematical. We have seen that for hot stars the polarization in at visible wavelengths is quite small, so until there is a space-based spectropolarimeter we should concentrate on the cooler stars.

As we see from Fig. 5, the expected polarization will be greater for stellar atmospheres of lower surface gravity. However, as stars evolve to the giant branch, their rotational velocity decreases due to the conservation of angular momentum. If the projected rotational velocity is less than the total (micro- plus macroturbulent) line broadening, the Öhman effect is very small (Fig. 14). There are some giant stars, however, with relatively high rotation (Tayar et al., 2015). It has been proposed that these stars have been spun up by the engulfment of a companion (Privitera et al., 2016).

It may be possible to increase the observability of the Öhman effect by noting that nearly the same Q/I profile will apply to all the lines in a section of the stellar spectrum. For example, consider the far UV lines shown in Fig. 11 and Fig. 12. We note that the same sort of Q profile corresponds to each strong line. Thus by binning the Stokes Q/I and U/I based on the location of the absorption features, we may be able to detect a faint polarization signal that could not be seen in a single line. Incidentally, the direction of such polarization would reveal the angle of the star's rotation axis projected on the plane of the sky.

8 July, 2016

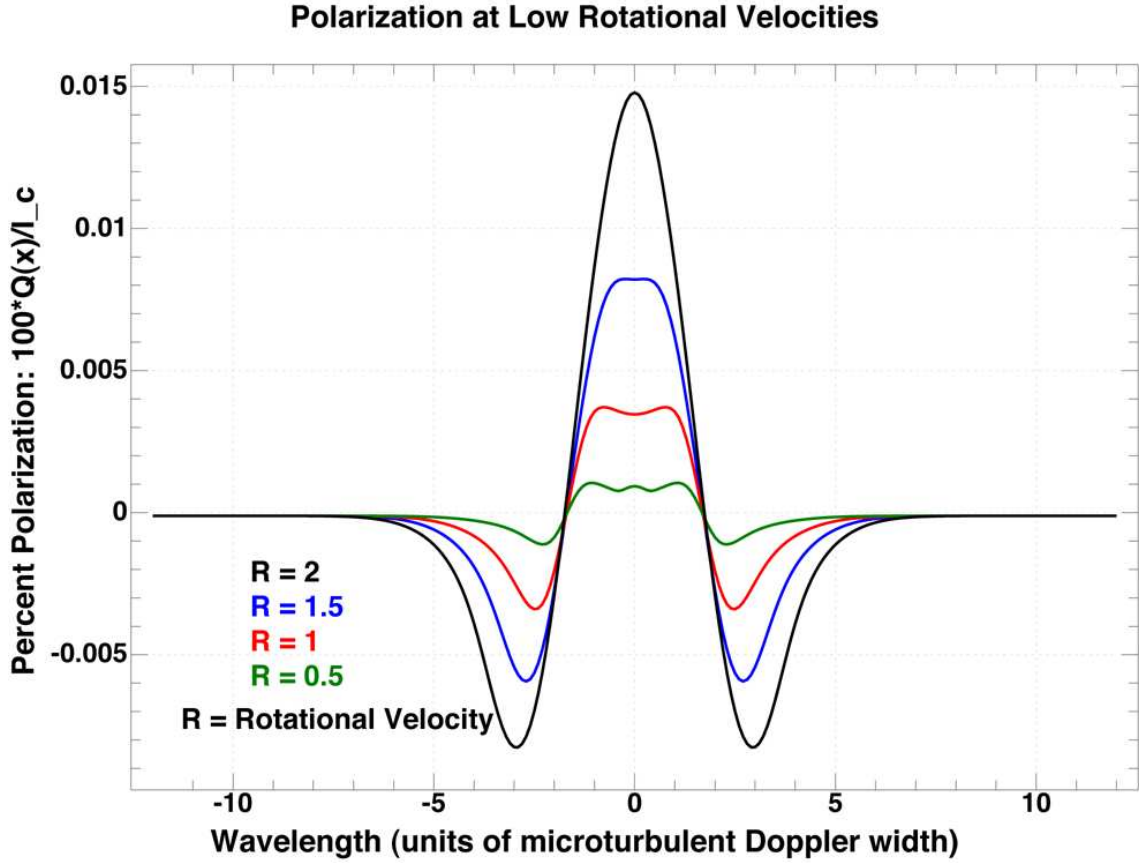


Fig. 14.— We show the Öhman effect polarization for a Milne-Eddington line in a $T=4000\text{K}$, $\log g=3.5$ (K giant) model atmosphere. The line is at 4000\AA with a line strength of $r_l = 10$. The microturbulent velocity is unity and the R-T macroturbulence has width $\zeta_{RT} = 2$. We show the percent polarization for four values of R , the maximum equatorial Doppler shift due to rotation. It is seen that if the rotation is only half the microturbulent line width ($R = 0.5$), the polarization drops to $\sim 10^{-5}$ (green profile).

REFERENCES

- Carciofi, A. C., and Magalhães, A. M., 2005, *Ap.J.*, **635**, 570.
- Chandrasekhar, S., 1946, *Ap.J.*, **103**, 351.
- Chandrasekhar, S., 1960, *Radiative Transfer*, Dover Publications, New York.
- Code, A. D., 1950, *Ap.J.*, **112**, 22.
- Collins, G. W. II, and Cranmer, S. R., 1991, *M.N.R.A.S.*, **253**, 167.
- Collins, G. W. II, Truax, R. J., and Cranmer, S. R., 1991, *Ap.J.Supp.*, **77**, 541.
- Gandorfer, A., 2002, *The Second Solar Spectrum*, Vol. II: 3910Å to 4630Å, Hochschulverlag AG an der ETH Zürich.
- Gray, D. F., 2005, *The Observation and Analysis of Stellar Photospheres*, 3rd edition, Cambridge University Press, Cambridge, UK.
- Harrington, J. P., 1969, *Ap. Letters*, **3**, 165.
- Harrington, J. P., 1970, *Ap. and Space Science*, **8**, 227.
- Harrington, J. P., 2015, in *IAU Symp. No. 305*, eds. K. N. Nagendra, S. Bagnulo, R. Centeno & M. Martinez Gonzales, p 395. (Cambridge University Press)
- Harrington, J. P., and Collins, G. W. II, 1968, *Ap.J.*, **151**, 1051.
- Kostogryz, N. M., and Berdyugina, S. V., 2015, *A& Ap*, **575**, A89.
- Kostogryz, N. M., Milic, I., Berdyugina, S. V., and Hauschildt, P. H., 2016, *A& Ap.*, in press. (arXiv:1511.07213)
- Öhman, Y., 1946, *Ap.J.*, **104**, 460.
- Privitera, G., et al., 2016, *A&A*, **591**, A45.
- Privitera, G., et al., 2016, *A&A*, in press (arXiv:1606.08027).
- Tayar, J., et al., 2015, *Ap.J.*, **87**, 82.